JOURNAL OF GEOPHYSICAL RESEARCH, VOL. 104, NO. C2, PAGES 3121–3132, FEBRUARY 15, 1999

# Diagnosing a meander of the shelf break current in the Middle Atlantic Bight

Robert S. Pickart, Daniel J. Torres, Theresa K. McKee, Michael J. Caruso, and Jennifer E. Przystup

Woods Hole Oceanographic Institution, Woods Hole, Massachusetts

**Abstract.** Two wintertime hydrographic crossings of the shelf break current in the Middle Atlantic Bight are analyzed. Separated by 3 days, the two sections sampled opposite phases of a meander of the current. The shipboard acoustic Doppler current profiler (ADCP) data reveal a strong, convergent jet during the first crossing, transporting 0.32 Sv of water equatorward. During the second crossing the transport is the same but the jet is weak and divergent. The measured Rossby numbers imply that the jet is significantly nonlinear in the convergent state. The associated potential vorticity $Q$ distributions differ substantially; the core of the weak jet is characterized by a region of uniform $Q$, whereas the strong jet contains no such feature. Surface thermal imagery indicates that the leading edge of a steep meander trough was sampled during the first crossing, followed by a broad crest during the second crossing. This is consistent with the convergent versus divergent nature of the flow in the two sections. A nearby Gulf Stream ring likely caused the steepening of the trough. After integrating the spatially low-passed thermal wind shear, the resulting geostrophic sections are compared to the similarly low-passed ADCP fields. This, together with the scales of the meander deduced from the surface imagery, indicates that the trough was in gradient wind balance, whereas the crest was predominantly geostrophic. These observations are consistent with the structure and dynamics of modeled baroclinic jets.

## 1. Introduction

The shelf break current of the Middle Atlantic Bight exhibits such complex, quickly evolving features that it is often difficult to obtain unambiguous measurements of the flow. Part of the difficulty is that the current is sensitive to numerous forcing mechanisms, all of which can significantly alter the configuration of the current. As a result, in situ measurements often catch only a glimpse of the behavior and evolution of the jet. Nonetheless, partly owing to the locus of such efforts, a clearer understanding is emerging of the current's structure, variability, and dynamics.

Because of the strong variability, it is difficult even to characterize the "undisturbed" basic state of the current. *Burrage and Garvine* [1988] present one mean view based on repeat hydrography, which nicely shows the summertime structure of the front. In their work, however, they point out the difficulty in interpreting a single synoptic section. This is partly due to the presence of high-frequency, superinertial motions, which can significantly alias synoptic scale measurements [see also *Burrage and Garvine*, 1987]. The most comprehensive mean view of the shelf break current is given by *Linder and Gawarkiewicz* [1998], who compiled all available hydrographic sections in the Middle Atlantic Bight between 1900 and 1990. The resulting mean fields quantitatively show the canonical summer and winter configuration of the front and jet (Figure 1). In wintertime the density front extends throughout the water column from the shelf break to the surface, whereas in summer a strong seasonal pycnocline develops isolating much of the front from the surface. *Beardsley and Flagg* [1976] nicely describe this seasonal evolution. The associated mean thermal wind fields from *Linder and Gawarkiewicz* [1998] imply that the jet is, on average, stronger in summer (Figure 1c).

It remains an ongoing goal to characterize and ultimately understand the variability associated with the jet. This, for example, will help toward quantifying the cross-frontal exchange of mass and properties. The basic state described above is baroclinically unstable [*Flagg and Beardsley*, 1978; *Gawarkiewicz*, 1991]. The jet also responds to local wind forcing [e.g., *Houghton et al*., 1988] as well as remote source water variations [e.g., *Chapman and Beardsley*, 1989; *Petrie and Drinkwater*, 1993]. Perhaps the biggest impact on the evolution of the jet, however, is from the surrounding slope water, particularly the presence of Gulf Stream eddies and rings [e.g., *Ramp et al*., 1983].

Despite the fact that there are so many factors exerting influence on the shelf break current, certain classes of frontal behavior are now fairly well established. For example, in the absence of rings the front is known to develop finite amplitude, westward propagating waves or meanders [*Burrage and Garvine*, 1988; *Beardsley and Flagg*, 1976]. These apparently develop into larger-amplitude, backward breaking waves, also called shelf break eddies [*Garvine et al*., 1988; *Houghton et al*., 1986]. It remains unclear how often such eddies actually detach from the front, though apparently this happens more frequently in summer [*Wright*, 1976]. When Gulf Stream rings approach the shelf break, the front can react in several ways. Streamers of shelf water often develop on the perimeter of the ring, leading to offshore transport [*Halliwell and Mooers*, 1979; *Joyce et al*., 1992]. The enhanced cross-stream gradients can also lead to energetic eastward propagating waves [*Ramp et al*.,

Copyright 1999 by the American Geophysical Union.

Paper number 1998JC900066.
0148-0227/99/1998JC900066$09.00

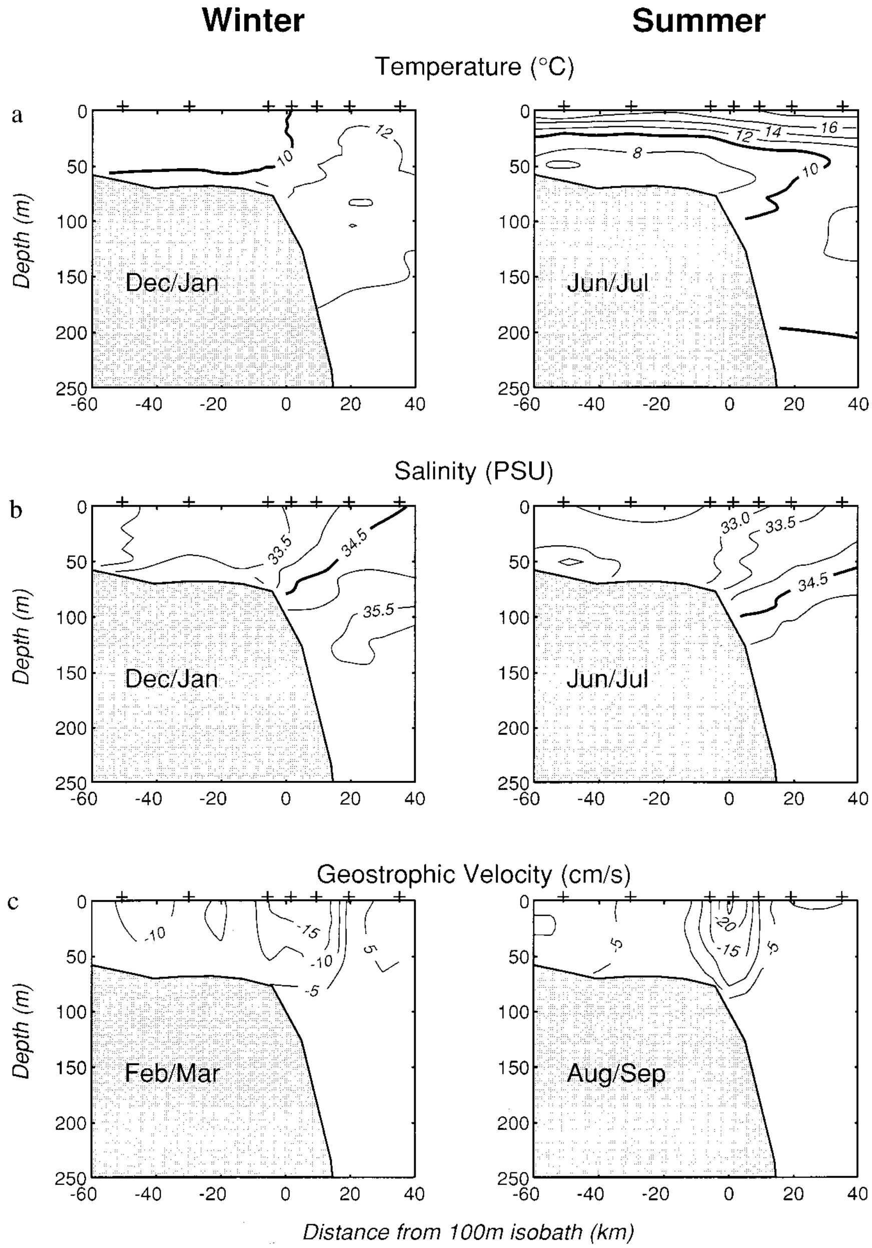


**Figure 1.** Mean winter and summer sections of (a) temperature, (b) salinity, and (c) referenced geostrophic velocity of the shelf break current [from *Linder and Gawarkiewicz*, 1998].

1983]. The nearby presence of the Gulf Stream itself can also strongly impact the front, causing complex exchanges of shelf and Gulf Stream water [*Gawarkiewicz et al*., 1996]. Finally, the shelf break current responds to local winds, and observations indicate that the jet fluctuates coherently over fairly large along-stream scales [*Houghton et al*., 1988].

Less is known about the dynamics that accompany the different types of shelf break current variability. The evolution of the front without external forcing (i.e., without rings, wind events, etc.) is likely due to baroclinic instability [*Gawarkiewicz*, 1991; *Morgan*, 1997]. The large-amplitude breaking waves (or shelf break eddies) that ultimately develop can be highly nonlinear. For example, *Houghton et al*. [1986] measured a Rossby number >0.7 associated with one such feature and suggested that the offshore flow of the eddy may be in gradient wind balance. Large Rossby numbers are regularly observed in the jet, particularly in the cyclonic shear zone [e.g., *Burrage and Garvine*, 1988; *Linder and Gawarkiewicz*, 1998]. *Spall* [1995] has studied the evolution and dynamics of baroclinic jets within the framework of a primitive equation model, investigating the process of eddy detachment. In subsequent work with an imposed external confluent flow [*Spall*, 1997], the jet develops breaking waves that are more reminiscent of the observed shelf break eddies. The cross-stream secondary circulation within these features consists of upwelling/downwelling cells, while the along-stream flow is in approximate gradient wind balance.

The work reported in this paper falls into the above mentioned category of only catching a glimpse of the frontal evolution. In fact, the observations presented here were not the major thrust of the cruise. However, there are several unique aspects that were revealed by our shelf break measurements that make them worth presenting. First, we show two highly resolved, unambiguous acoustic Doppler current profiler (ADCP) velocity realizations of the shelf break jet, clearly revealing its two-dimensional structure. These are the first of their kind reported in the literature. Second, these transects were taken during a time period when the front contained westward propagating waves or meanders (i.e., prior to fully developed shelf break eddies), and we sampled two different phases of a meander. Last, we quantitatively compare the thermal wind fields to the full velocity fields and discuss the probable ageostrophic dynamics involved.

## 2. Fieldwork

From December 5–10, 1995, the initial field phase of the Shelf Break PRIMER experiment was carried out aboard R/V *Endeavor*. PRIMER is a coordinated, multi-institutional effort to investigate both the acoustics and the physical oceanography of the shelf break front in the Middle Atlantic Bight. The experiment included two intense field phases, one in summer 1996 and one in winter 1997, employing acoustical arrays and SeaSoar measurements in the frontal region. Part of the focus of PRIMER includes investigation of the coupling between the front and adjacent slope water, and toward this end a long-term moored array was set in the shelf break current and adjacent slope water prior to the two major field surveys. The deployment of this array was the primary purpose of the 6-day 1995 *Endeavor* cruise.

Before setting the array, a high-resolution expendable bathythermograph (XBT)/shipboard ADCP survey was carried out across the shelf break front, partly to obtain an accurate bathymetric profile. The survey took approximately 6 hours. At the conclusion of the mooring work the XBT line was reoccupied using a Mark III conductivity-temperature-depth (CTD) (using the same 3.7-km spacing; see Figure 2). The second crossing took 13 hours. It is these two sections that are reported on here, separated by approximately 3 days. The velocity structure of the jet is vastly different in the two occupations.

The CTD data were averaged into 2-dbar bins. Comparison of the precruise and postcruise laboratory calibrations for temperature and conductivity indicate an accuracy of better than 0.001°C for temperature and 0.02 practical salinity units (psu) for salinity. The XBT data were despiked and decimated every 5 m; the accuracy of the thermistor probe is 0.1°C. The shipboard ADCP was a narrowband 150-kHz unit mounted on the hull at 5 m depth. These data were averaged into 5-min ensembles with a 4-m bin depth and processed with the Common Oceanographic Data Access System (CODAS) software package (E. J. Firing et al., unpublished manual, 1995). The shallowest depth bin is centered at 15 m, and the region of good data extends to about 85% of the water depth. The lateral resolution on the first crossing was approximately 1.5 km and even better on the second crossing (though it was subsequently interpolated to match that of the first section).

Sources of error in the shipboard ADCP measurements are due primarily to instrument error and from converting the measured velocity into absolute velocity. The former is primarily due to scatter of the acoustic pulses and speed of sound variations at the transducer. Using ensemble averaging and calibrated speed of sound (from the shipboard thermosalinograph and CTD stations) greatly reduces the relative velocity error to as low as 1 cm/s. Transforming the measured velocity into absolute velocity includes error from misalignment of the transducer, ship heading inaccuracies (three-dimensional Global Positioning System (GPS) was not available on the cruise), and ship speed error due to the differential GPS scatter. Both water- and bottom-track methods were used to correct for the transducer misalignment, which was found to be −3.9°. This agrees quite well with a similar calibration performed on an earlier *Endeavor* cruise. The ship speed correction was determined using *Endeavor*'s differential GPS. A previous dockside test of this instrument quantified the associated rms error, which was quite small (±3.5 m). For the 5-min ensemble averaging the associated velocity error is estimated to be of the order of 2 cm/s. We were unable to correct for the ship's gyro error with any confidence. While the short-term gyro fluctuations are reduced by the temporal filtering in CODAS, any long-term biases remain. However, the overall consistency of the ADCP fields and associated transports presented in section 3 attest to the smallness of any such error.

We did not correct the velocity data for tides. It should be remembered, however, that during the winter season (without a shallow pycnocline present) the baroclinic tides will be reduced. According to *Moody et al.* [1984], the zonal tidal amplitude at 30 m near the location of our transect, in the water depth where we observed the jet, is approximately 5 cm/s. This

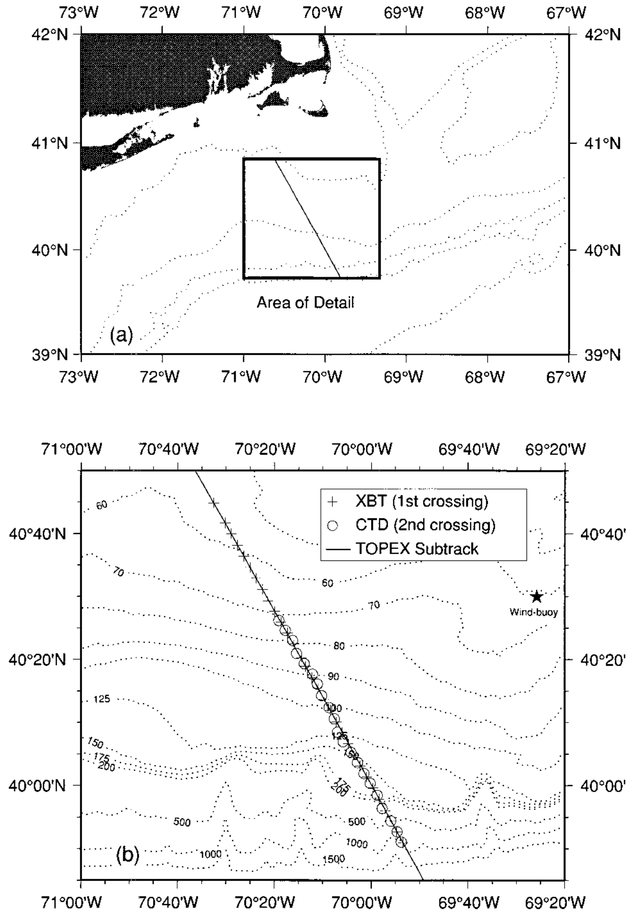


**Figure 2.** (a) Region of the Shelf Break PRIMER experiment, south of Cape Cod, Massachusetts. The displayed isobaths are 50, 100, 1000, 2000, and 3000 m. (b) Detailed view of the two hydrographic crossings along the TOPEX altimeter line and the bathymetry of the shelf and slope. The location of the Nantucket wind buoy is indicated as well.

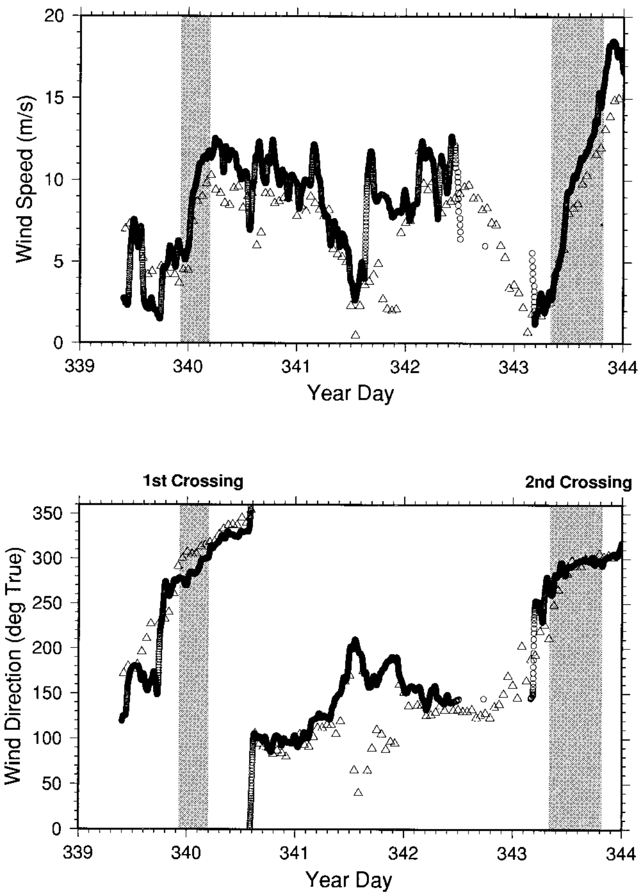


**Figure 3.** Time series of (top) wind speed and (bottom) wind direction (plotted in the oceanographic convention). Circles denote the shipboard data (corrected for motion of the ship) and triangles are from the nearby Nantucket wind buoy. The time periods of the two shelf break hydrographic crossings are indicated by the shading.

is 10–15% of the observed core speed of the jet and hence does not significantly impact any of our conclusions. To verify this further, we computed the $M_2$ tidal amplitude from one of the PRIMER shelf break ADCP moorings (located at 168 m depth just shoreward of the shelf break) deployed during the cruise. The autospectrum of the zonal velocity computed for the December–January time period showed little variation throughout the water column. The associated mean tidal amplitude was 5.1 cm/s, with a 95% confidence interval of 1.7 cm/s. This is consistent with the *Moody et al.* [1984] value. Internal tides also impact the vertical displacement of the shelf break density front. The horizontal wavelength of the first baroclinic mode of the internal tide was estimated using a simple, linear, flat-bottom model (J. Colosi, personal communication, 1998). Using a buoyancy-frequency profile at the center of the jet from the second crossing, the wavelength was found to be 25 km. Hence this should not influence the overall tilt of the shelf break front seen in the CTD fields.

In situ winds were measured during the cruise using an anemometer located approximately 10 m above sea level. These data were converted to absolute winds using the navigation data and smoothed using a 1-hour filter. The Nantucket wind buoy is located roughly 75 km to the east of our shelf break section (Figure 2), which also provided a time series of hourly winds 5 m above sea level. Overall, the agreement between the two data sets is quite favorable (Figure 3). During both of the shelf break crossings the winds were directed from the east (or toward the west as in Figure 3), steadily increasing in strength. However, for the majority of the time period between the two surveys, the wind was predominantly toward the southeast (Figure 3). The average wind stress over this period was 1.3 dyn/cm$^2$, which implies an average offshore Ekman velocity of 4.8 cm/s over the depth of the mixed layer (~25 m). We believe that the observed evolution of the jet between the two crossings was not a result of the local winds. This idea is reinforced by examining the movement of the surface front over this time period, which is opposite of the sense suggested by wind forcing alone (section 4).

## 3. ADCP Crossings

The hydrographic transect (Figure 2) is not oriented normal to the mean angle of the bathymetry, as is typically the case for shelf break sections. This is because the PRIMER experiment included a remote sensing component, and it was decided beforehand to situate the long-term moored array along a subtrack of the TOPEX altimeter. The reasoning was that the in situ measurements might help ground truth the sea surface height data (including removal of the tidal signal). Thus the associated hydrographic crossings were also done along the TOPEX line.

Because of this, we employ a coordinate frame that is normal to the local angle of the isobaths (where the rotation angle varies as a function of along-track distance). A right-handed system is used where positive $y$ and $v$ are along-isobath distance and velocity, respectively, in the equatorward direction and positive $x$ and $u$ are offshore distance and velocity, respectively. In order to do this, we required accurate bathymetry of the region. U.S. Geological Survey (USGS) soundings data were obtained for the PRIMER area, which were subsequently interpolated to a regular grid of 0.02° resolution (2.2 km). The resulting bathymetric contours appear to be quite accurate. We compared closely the sounding depth along the TOPEX line to that obtained using *Endeavor*'s chirp sonar during the XBT survey, and the agreement was excellent. There is also favorable agreement between the soundings and the available General Bathymetric Chart of the Oceans (GEBCO) data in the region. To determine the appropriate coordinate rotation angle, a two-dimensional spline was fit to the USGS bathymetry grid (after smoothing it with a Laplacian filter). This provided a functional relation between local isobath angle and station position along the transect.

The along-isobath ADCP velocity computed as such clearly reveals the shelf break current in both crossings, though the jet structure is substantially different in the two realizations (separated by roughly 3 days; see Figure 4a). The jet is much stronger and narrower in the first crossing on December 6; the peak velocity is 66 cm/s and the $e$-folding width is 15 km. On December 9 the jet is located 5 km farther onshore and has a peak velocity of only 36 cm/s and width of 25 km. The transport, however, has remained the same (computed over the $e$-folding width and to 100 m depth) and is 0.32 Sv in both realizations. This is comparable to the December/January climatological mean value for the region considered by *Linder and Gawarkiewicz* [1998] that encompasses the PRIMER line. (Both the winter transport value quoted by *Linder and Gawarkiewicz* [1998] as well as the estimate presented here

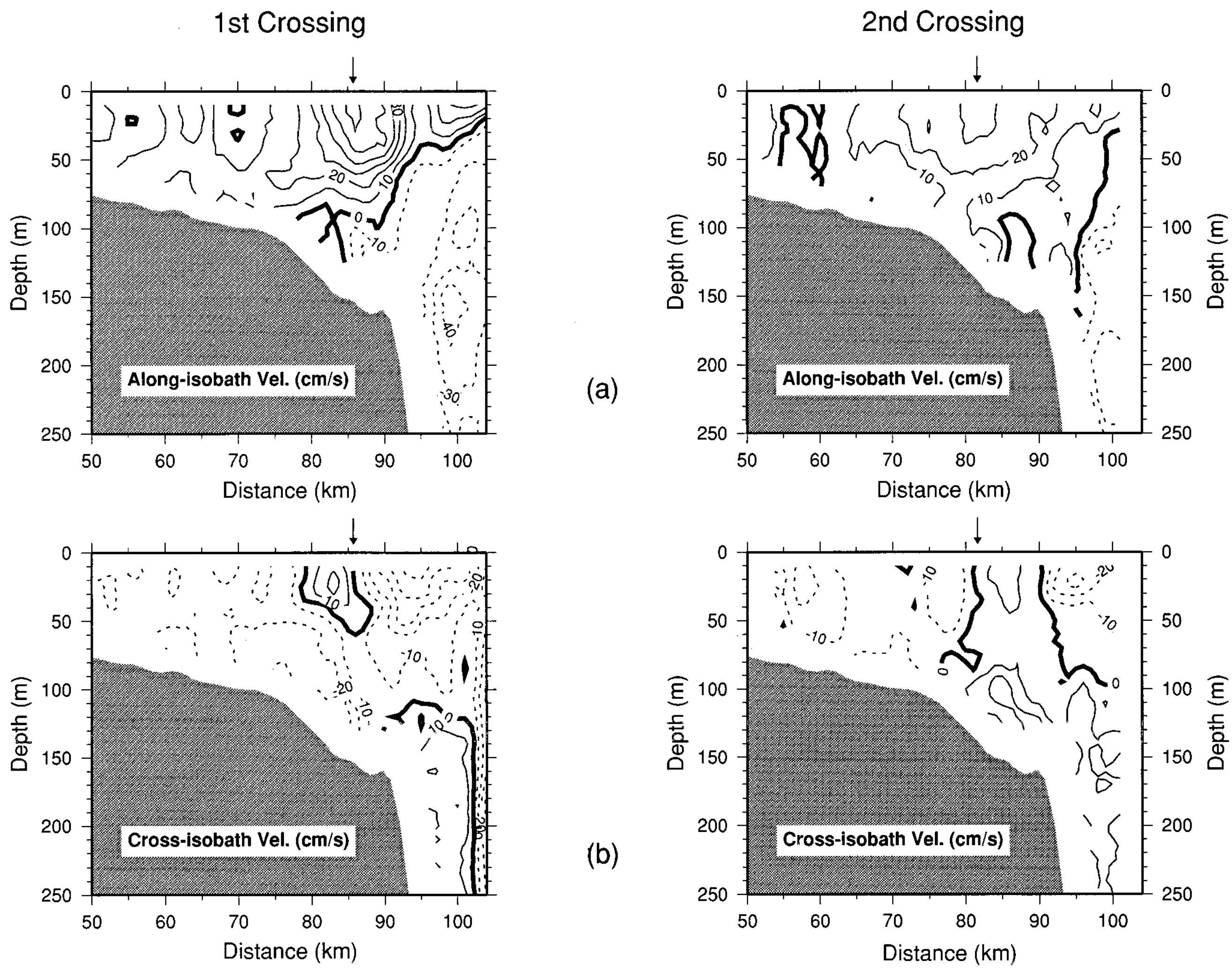


**Figure 4.** (a) Along-isobath and (b) cross-isobath velocity of the shelf break jet from the shipboard acoustic Doppler current profiler (ADCP) for the two different crossings. The axis of the jet is marked by the arrow. Positive flow (solid contours) is equatorward/offshore.

were computed over the full vertical extent of the jet and across an $e$-folding lateral scale.) Note the region of eastward flow beneath the seaward edge of the jet in the first crossing, which becomes more intensified farther downslope. This is Gulf Stream ring water (see next section), which had largely disappeared by the time of the second crossing. While the nearby ring did not disrupt the westward flow of the jet, the ring played an important role in the behavior of the shelf break current meanders during this time period (section 5).

The cross-isobath flow (Figure 4b) reveals an interesting symmetry between the two realizations of the jet. In the first crossing the shelf break current is strongly convergent, with the core of the jet flowing parallel to the bathymetry. Three days later, the jet is weakly divergent, but again, the core is aligned with the isobaths (even though the jet has moved to shallower depths, where the bathymetry is oriented at a different angle). One wonders if the jet is dynamically responding to the local bathymetry as it meanders or if this is just coincidence. It is clear, however, that the jet evolves from a strong/convergent state to a weak/divergent one, which is reminiscent of the jet variability discussed by *Spall* [1997] and similar as well to the structure observed in Gulf Stream meanders [e.g., *Hummon and Rossby*, 1998]. This pattern, together with the satellite imagery presented in section 5, implies that we observed two different phases of a meander of the shelf break current. The difference between the two jet states is also nicely visualized in the depth-integrated ADCP vectors (Figure 5), which clearly show the convergence and divergence noted above.

As is true with most of the measurements of the shelf break current, the cross-stream shear in velocity on the offshore side of the jet is stronger in both our sections. In the first crossing the narrowness of the core leads to a Rossby number $\zeta_{max}/f \sim 0.7$ (where $\zeta_{max}$ is the relative vorticity in the high cyclonic shear region and $f$ is the Coriolis parameter). By contrast, $\zeta_{max}/f \sim 0.3$ in the second crossing. This suggests that the jet may be nonlinear in the convergent state but essentially linear in the divergent realization.

It is of interest to determine the impact of these values of relative vorticity versus layer-thickness changes on the potential vorticity structure of the current. Because the stratification is weak in winter, one might expect the jet to be sensitive to the presence of the bottom (the alignment of the jet core with the bathymetry noted above gives this impression as well). The potential vorticity was calculated as $Q = (f + \zeta)/h$, where $\zeta$ is the average relative vorticity over the vertical extent of the jet and $h$ is the water depth. We are justified in considering this

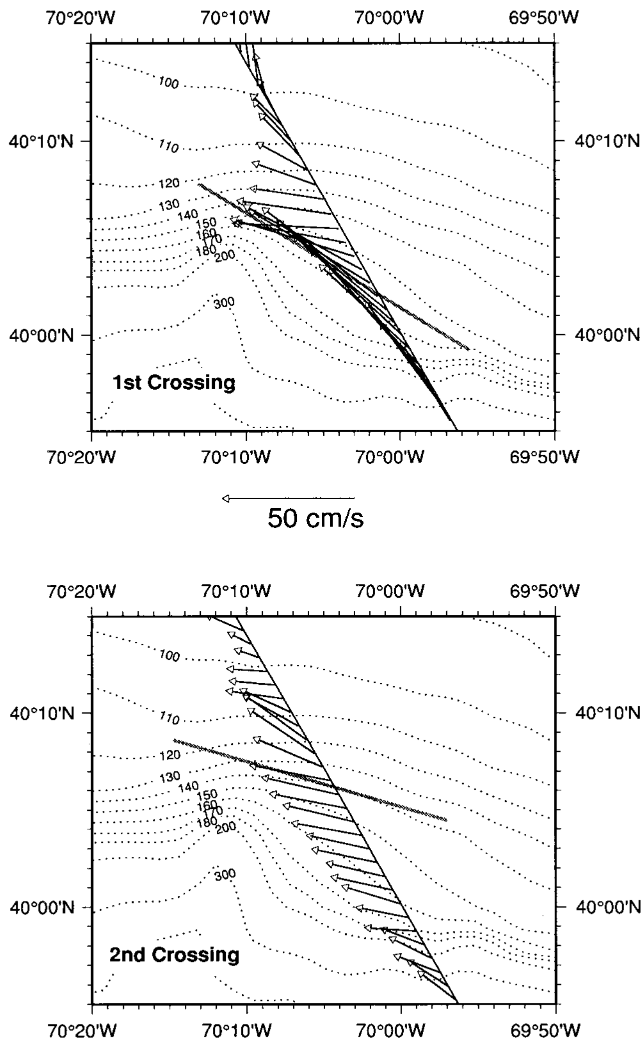


**Figure 5.** Integrated ADCP velocity over the depth range 0–60 m for (top) first and (bottom) second crossings. The gray line marks the center of the jet in each crossing, oriented in the direction of the mean current.

single-layer representation of $Q$ because of the large vertical penetration height implied by the scales of the current. The penetration height is given by $D = Lf/N$, where $N$ is the buoyancy frequency and $L$ is the width of the current. From our measurements, $N \sim 10^{-2}$ s$^{-1}$, $L \sim 20$ km, and $f \sim 10^{-4}$ s$^{-1}$, hence $D \sim 200$ m. This is greater than the water depth where the jet resides, implying that the shelf break current should indeed feel the bottom.

Not surprisingly, the cross-stream distributions of $Q$ for the two crossings are quite different (Figure 6). When the jet is strong, the potential vorticity structure is dominated by the variation in $\zeta$. This is demonstrated by computing the potential vorticity using a uniform bottom depth (the value at the center of the jet $H$). This quantity does not differ substantially from $Q$ within the jet (on the outer edges, $Q$ approaches $f/h$; see Figure 6a). The two extrema in $Q$ on either side of the jet axis are due to the large changes in relative vorticity there. This should be contrasted to the potential vorticity structure when the jet is weak (Figure 6b). Here the variation in bottom depth is as important as the change in $\zeta$, which results in a region of uniform potential vorticity in the center of the jet. These results have important ramifications. When the jet is predominantly linear, the potential vorticity may be modeled as a uniform value (e.g., as in the work by *Condie* [1993]). However, in the nonlinear state as sampled during the first crossing, the potential vorticity structure varies strongly across the jet.

## 4. Hydrographic Crossings

The first occupation of the shelf break current consisted of XBT measurements, which clearly reveal the temperature front (Figure 7a). Note the absence of the seasonal thermocline, which has eroded by December. The water on the shelf is well mixed (though the foot of the front has a shoreward extension), and seaward of the front is a region of warm water centered at roughly 80 m depth. These features are qualitatively similar to the climatological mean December/January section of *Linder and Gawarkiewicz* [1998] in this region (Figure 1a). The second occupation was done using a CTD, and the temperature section has the same overall structure as the first crossing (the warm region offshore has diminished somewhat; see Figure 7b). (For the rest of the paper we employ an along-

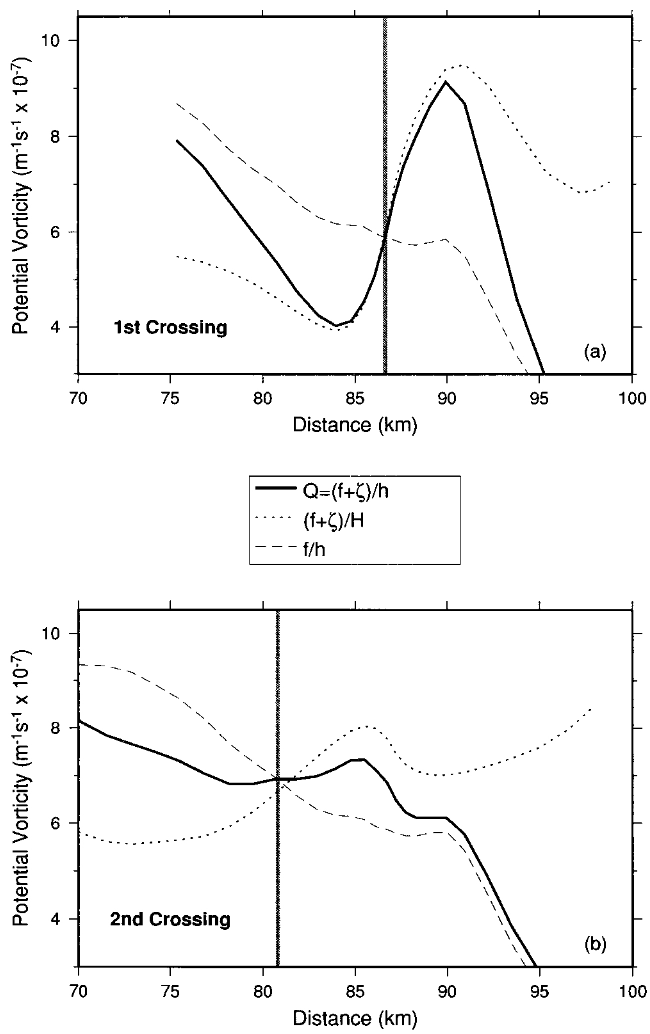


**Figure 6.** Low-passed distribution of potential vorticity (solid line) compared to that using a constant bottom depth (dotted line) and that containing no contribution from the relative vorticity (dashed line). The location of the jet axis is marked in each case by the vertical gray line.

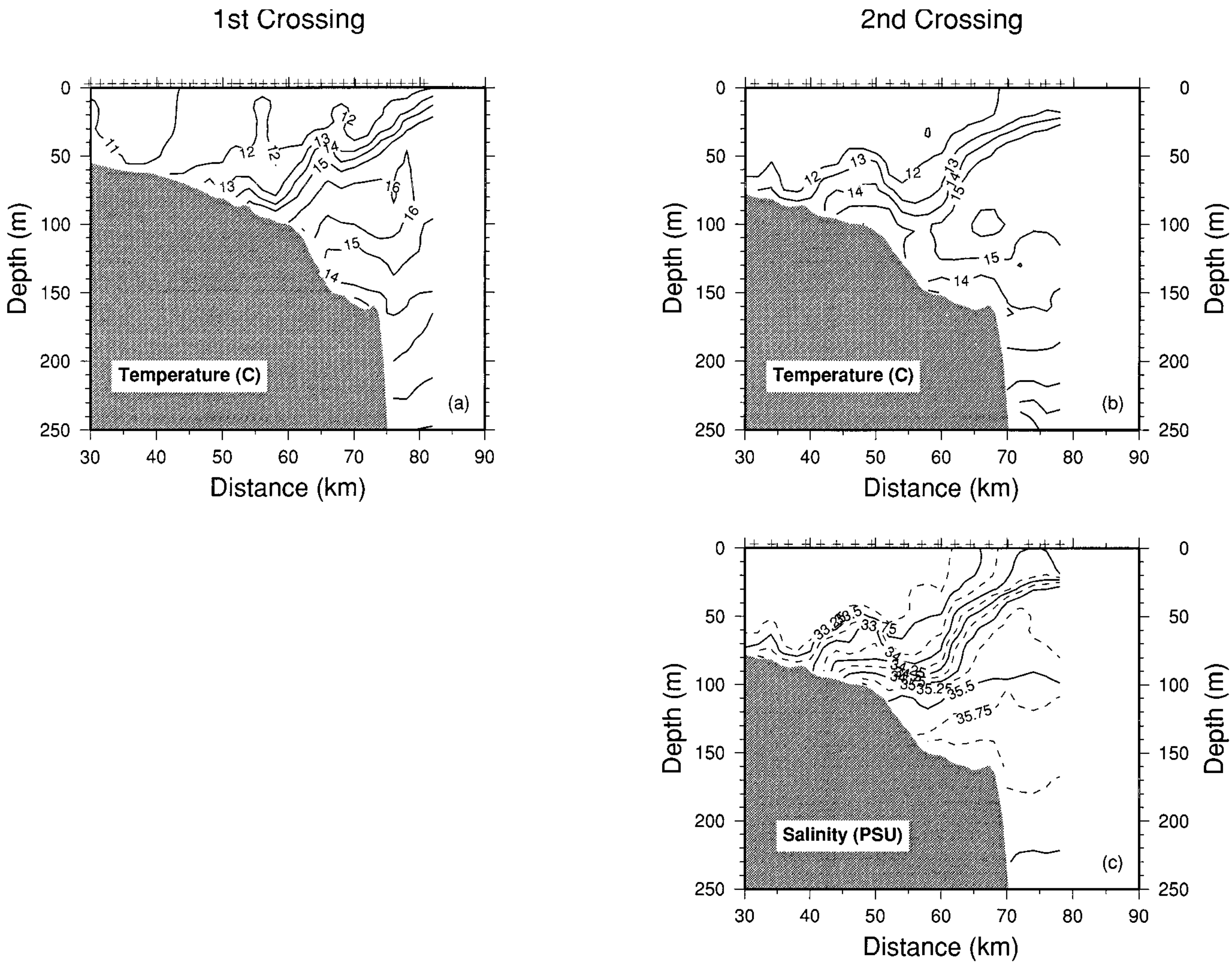


**Figure 7.** Hydrographic transects across the jet (with station positions marked by crosses). (a) Expendable bathythermograph (XBT) temperature of the first crossing. (b) Conductivity-temperature-depth (CTD) temperature of the second crossing. (c) CTD salinity of the second crossing.

stream/cross-stream coordinate system, where the orientation was determined by the direction of the mean current in the two crossings, as revealed by the ADCP velocities (see Figure 5). Positive along stream is equatorward; positive cross stream is offshore.) The salinity field reveals the presence of Gulf Stream ring water near the bottom (salinities >35.5 psu; see Figure 7c). As discussed earlier, this was expected based on the eastward flow at these depths in the ADCP sections and the nearby presence of the ring.

Note the difference between the surface outcrop of the 12°C isotherm between the two sections (Figure 7a versus 7b). One possible explanation for this could be that the near-surface front was advected by Ekman flow resulting from onshore favorable winds [e.g., *Ou*, 1984]. However, recall that during the period leading up to the second crossing the winds were offshore favorable (Figure 3), thereby discounting this possibility. More likely, the near-surface difference between the sections is caused by local convection. The heat loss associated with the strong winds (near 10 m/s; see Figure 3) and cold air (decreasing to 6°C) would tend to result in overturning. This would bring up warmer subsurface water, which in turn could result in the apparent onshore translation of isotherms. Over the 3-day period a mixed layer did indeed develop in the frontal region (see also Figure 9, top), consistent with such an explanation.

Because of the large differences in the directly measured velocity structure of the jet between the two crossings, we felt it would be revealing to compare the density structure as well. For instance, this would enable us to investigate the thermal wind field associated with the two states of the jet. Consequently, we carefully scrutinized the CTD data from the second crossing in order to determine a suitable $T$-$S$ relationship to apply to the XBT temperature data of the first crossing. The resulting synthesized salinities could then be used to determine density and hence the geostrophic velocity of the jet in the strong state.

The $T$-$S$ diagram for the entire set of CTD stations (second crossing; see Figure 8a) shows a well-behaved pattern with a sharp bend near $\sigma_\theta = 26.2$ kg/m$^3$. This corresponds to approximately 100 m depth, which is the vertical extent of the jet (Figure 4). Below this depth resides the ring water (Figure 7c), which has a different $T$-$S$ structure. Thus we considered only that part of the water column above $\sigma_\theta = 26.2$ kg/m$^3$ containing the front/jet. There are various ways one might construct a $T$-$S$ relation for this locus of points; we considered three (Figure 8a). The simplest approach is a polynomial fit (in this case

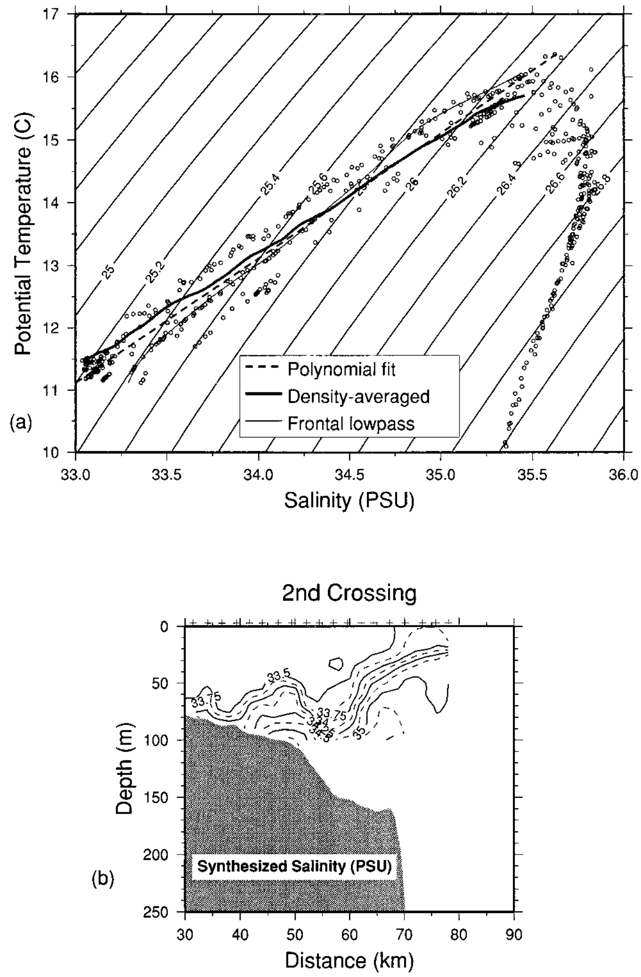


**Figure 8.** (a) $T$-$S$ scatterplot from the CTD data, including the various relationships discussed in the text (section 4). (b) Salinity of the shelf break front for the second crossing, derived from the CTD temperature data using the frontal low-pass $T$-$S$ relationship.

a linear and quadratic fit are nearly identical); another approach is to average the values on density surfaces. As a measure of the success of a given method, we can apply the relation to the temperature data of the second crossing and compare the result to the CTD salinity section (Figure 7c). Both of the above approaches result in good overall agreement. However, in each case the lateral salinity gradients in the center of the front are somewhat large, which in turn leads to an overestimation of the geostrophic core speed of the jet (i.e., compared to that calculated using the CTD sections of Figure 7). Since we are interested in quantitatively comparing the thermal wind fields to the ADCP velocities, we tried a third approach.

Because the bulk of the geostrophic shear of the shelf break current during winter is due to the front (since there is no seasonal pycnocline present), it is most important to determine salinity accurately in the frontal zone. Thus we constructed another $T$-$S$ relation using just those CTD stations in the center of the front (note that the front consists of the same isotherms in both crossings). In particular, we computed a low-pass curve using this subset of points, called the frontal $T$-$S$ relation, which differs from the above mentioned $T$-$S$ curves, particularly for temperatures $\geq$14°C (Figure 8a). For a given value of $T$ in this range, which occurs on the seaward edge of the front, the frontal $T$-$S$ curve returns a lower value of salinity and density, hence a weaker cross-stream density gradient. As expected, the resulting salinity field agrees quite nicely with the CTD section within the frontal zone (compare Figures 8b and 7c), though the agreement is generally worse over the rest of the section. However, as mentioned above, we are interested in accurately determining the jet's thermal wind shear. For the frontal $T$-$S$ relation the strength of the resulting geostrophic jet is within 5% of that resulting from the original CTD density section, whereas the other two $T$-$S$ methods overestimate the jet strength by more than 20%.

Using the frontal $T$-$S$ relation derived from the second crossing, we computed a synthesized salinity and density section corresponding to the first XBT crossing. This results in a density inversion offshore of the front, so we restricted our analysis to the frontal zone only ($25.5 \leq \sigma_\theta \leq 26.0$, Figure 9, top).

## 5. Ageostrophic Signal

### 5.1. In situ Measurements

It has been shown that high-frequency variability (tidal and supertidal) can significantly alias synoptic measurements taken in the vicinity of the shelf break in the Middle Atlantic Bight. In a summertime experiment, *Burrage and Garvine* [1987] found that tidally generated solitons can displace isopycnals by as much as 10 m, with horizontal wavelengths of <1 km and periods of the order of 15 min. The associated cross-shelf currents are significant as well. These structures are predominant in the seasonal pycnocline, and owing to the strong density gradients there, the potential for aliasing is particularly large. Our wintertime sections differ from the conditions encountered by *Burrage and Garvine* [1987, 1988], in that the seasonal pycnocline is absent and the vertical shear of the jet is predominantly due to the shelf break front itself. The physical nature of the two ADCP crossings (Figure 4) leads us to believe that the ADCP velocity fields presented in section 3 are not significantly degraded by aliasing due to short-period fluctuations.

The density structure, however, is clearly more sensitive to such high-frequency variability. The vertical sections (Figure 9, top) show small-scale vertical undulations of the density front, which are common in this region. The associated thermal wind fields would in fact result in narrow regions of poleward flow, obviously not associated with the shelf break jet. We therefore employed a spatial low-pass filter along the frontal isopycnals, using a filter width of 25 km. This is the characteristic wavelength of the undulations determined visually from Figure 9 (top), and also the estimated horizontal wavelength of the dominant internal $M_2$ tide as discussed in section 2. The resulting smoothed density sections (Figure 9, bottom) clearly show the structure of the front over the lateral scale of the shelf break jet and allow us to compute an unambiguous (albeit smoothed) geostrophic velocity field.

We are interested in carefully comparing the geostrophic signal of each state of the jet with the full velocity measurement provided by the ADCP data. Accordingly, we computed the along-stream ADCP velocity for each crossing, then smoothed these fields using a Laplacian spline filter equivalent to that used on the isopycnals (since it is inappropriate to compare smoothed thermal wind fields to unsmoothed ADCP fields). Furthermore, for each crossing we referenced the ther-

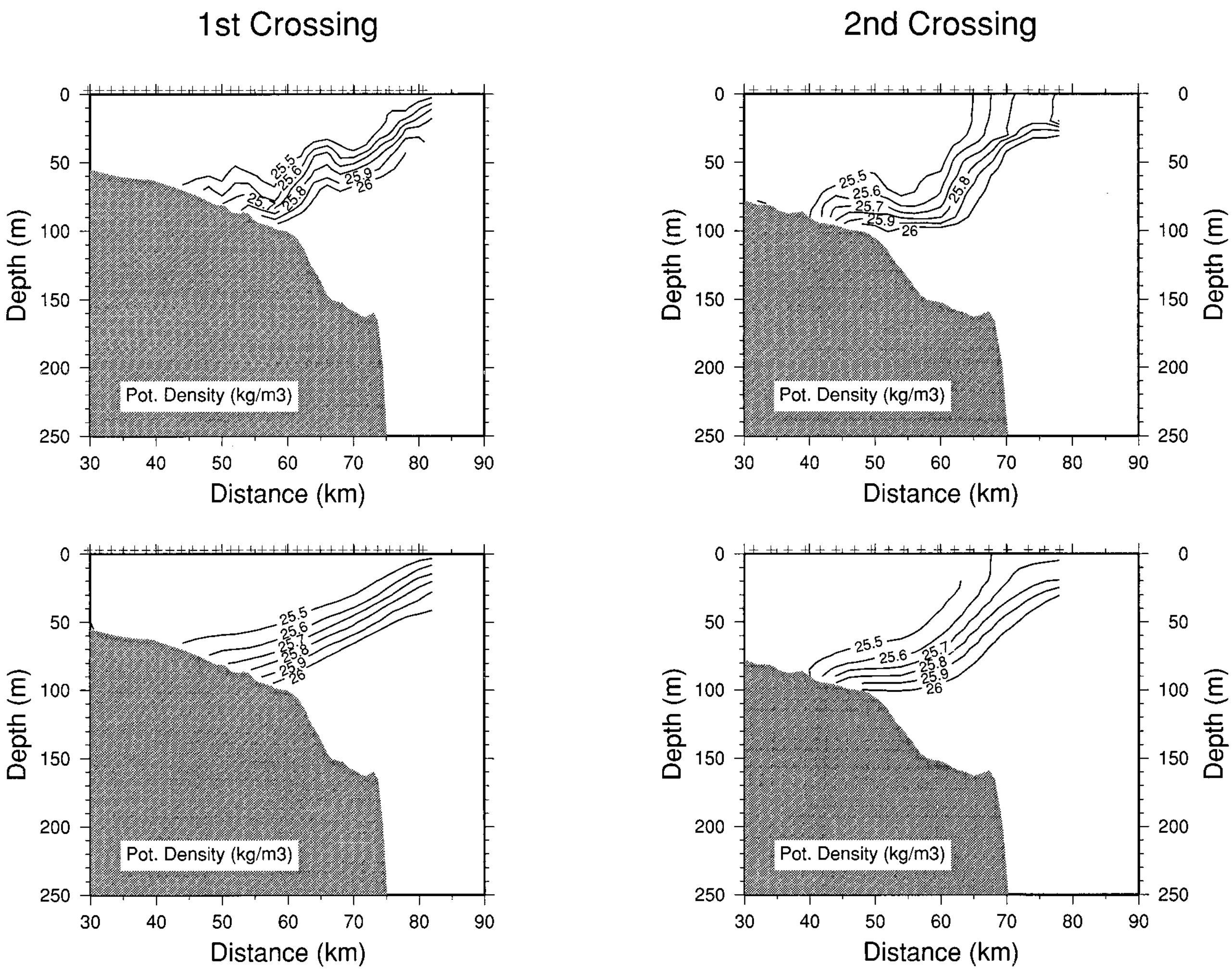


**Figure 9.** (top) Density of the shelf break front during the two transects. (bottom) Low-passed density front as described in the text (section 5.1).

mal wind field to the ADCP velocity along the $\sigma_\theta = 26.0$ surface, the argument being that at the base of the jet the flow should be in geostrophic balance. We believe that these steps lead to the most accurate comparison. The results indicate that during the first crossing the ADCP signal is a factor of 2 larger than the geostrophic signal, whereas during the second crossing the two signals are comparable (Figure 10). Thus, on the basis of our best interpretation of the observations, the conclusion is that the weak jet is geostrophically balanced, while the strong jet is significantly nonlinear. This is consistent with the large difference in Rossby numbers between the two states (section 3).

### 5.2. Remote Sensing

Is the observed discrepancy between geostrophy and the ADCP-measured core speed during the first crossing consistent with what is known about the dynamics of meandering jets? In *Spall*'s [1997] primitive equation model, whose lateral scales apply roughly to the shelf break current, the flow near the leading edge of meander troughs is convergent, while for crests it is divergent. This is true as well in the Gulf Stream, where numerous observations have revealed such a pattern [e.g., *Bower*, 1989; *Hummon and Rossby*, 1998]. For large enough Rossby number the momentum balance normal to the flow is that of gradient wind [*Holton*, 1979],

$$v^2/R + fv = fv_g, \tag{1}$$

where $v$ is the along-stream current, $R$ is the radius of curvature, and $v_g$ is the geostrophic signal. In troughs ($R < 0$) the gradient flow is greater than the geostrophic flow ($v > v_g$), while the opposite is true in crests. This balance has been shown to apply in the near-surface portion of the Gulf Stream [*Johns et al.*, 1989] and is appropriate as well for the meanders in the model of *Spall* [1997]. In our first crossing, $v > v_g$ when the flow is strongly convergent (Figure 4), which is consistent with these results. To determine if the magnitude of this measured ageostrophic signal is plausible, we analyzed the available advanced very high resolution radiometer (AVHRR) data encompassing the time period of the cruise.

A series of three sea surface temperature (SST) images taken prior to our first crossing (Plate 1) clearly shows the evolution of the shelf break front and the influence of the nearby Gulf Stream ring. (Except for two other images in late November, these are the only ones available for the 3-week period centered on the cruise.) The clearest image of the ring (Plate 1b) shows it centered near 39°15 N, 70°15 W (denoted R

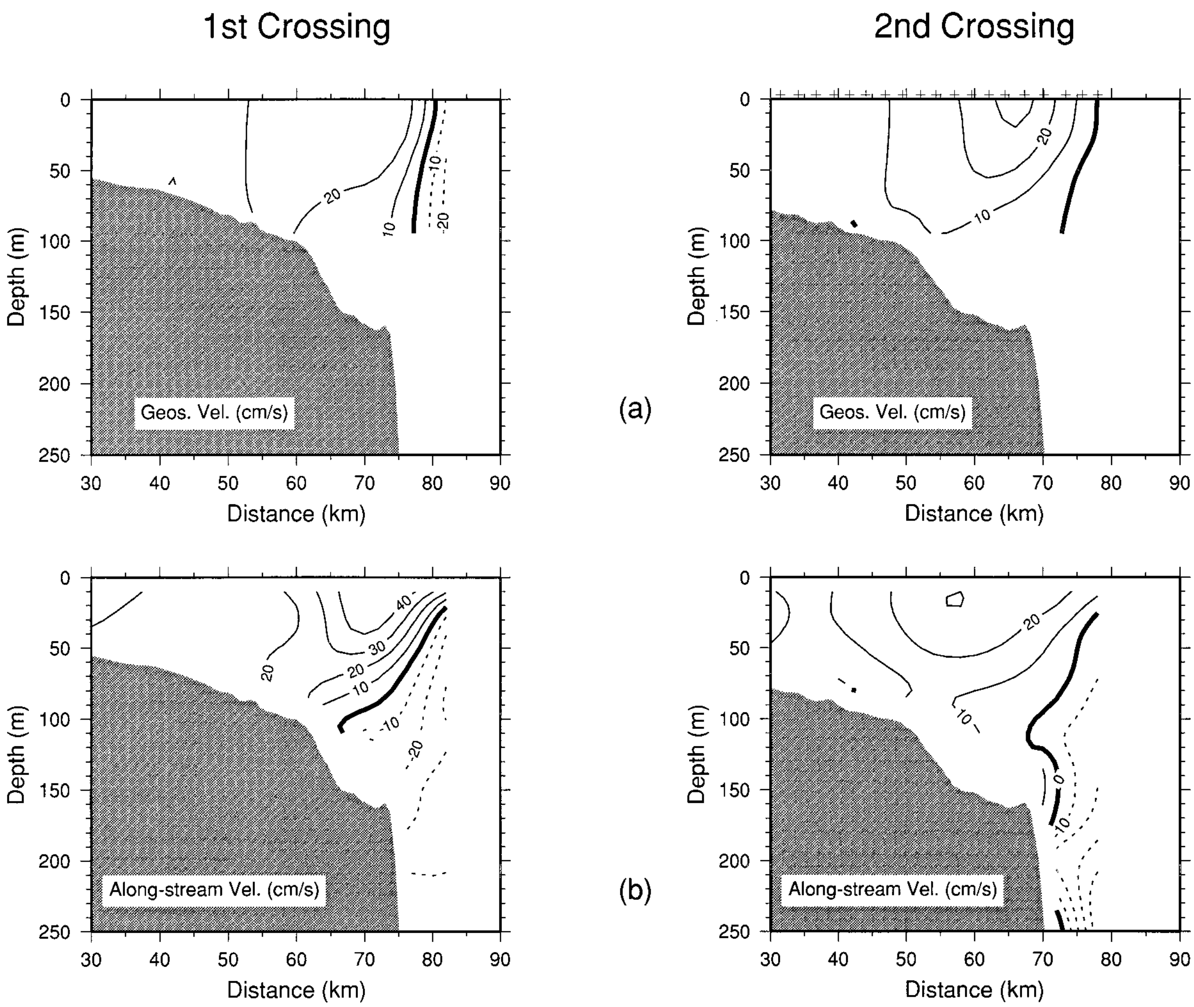


**Figure 10.** (a) Referenced geostrophic velocity of the jet (along $\sigma_\theta = 26.0$) compared to the (b) ADCP velocity section for each crossing.

in the plate). West of our section (away from the ring), the westward propagation of frontal shelf break meanders is clearly evident in the first two images (compare Plates 1a and 1b in the vicinity of 71.5–72.5°W). By applying simple feature tracking to these two realizations as well as to the pair of late November images (not shown), we obtain a propagation speed of 40 cm/s and 23 cm/s, respectively. These values are larger than predicted by baroclinic instability models [*Gawarkiewicz*, 1991; *Morgan*, 1997], though they are within the range observed by *Halliwell and Mooers* [1979] in the Middle Atlantic Bight. In Plate 1a, note the trough located to the east of our section (labeled T in Plates 1a–1c). In the days leading up to the cruise this feature steepens as it moves slowly westward (i.e., more slowly than the meanders farther west downstream of the ring). Both the steepening and slowness of propagation are most likely due to the presence of the ring.

Our first crossing occurred roughly 15 hours after the image in Plate 1c. It is clear that we sampled the leading edge of this deep trough, consistent with the strong convergence we measured in the velocity field (Figures 4 and 5). Inserting the measured values of $v$ (40 cm/s) and $v_g$ (20 cm/s) from Figure 10 into (1) implies a radius of curvature of 9 km. From the December 5 image (Plate 1c) the measured radius is 11 km. Thus the predicted and observed values of $R$ are comparable, suggesting that the flow is indeed in gradient wind balance in the trough. Plate 1c shows that following the trough is a broad crest (labeled C), which is likely what we measured during the second crossing 3 days later (the implied propagation speed is 15 cm/s, which is quite reasonable). This is both consistent with the weaker, divergent jet observed during that time (Figure 4) and the fact that the flow is geostrophically balanced (Figure 10). From the December 5 image, $R$ is of the order of 75 km for this crest, implying that $v$ and $v_g$ should agree within 30%. This is again consistent with our observations. Thus, in contrast to the steep trough of the first crossing, the flow in the trailing crest does in fact appear to be in approximate thermal wind balance.

Finally, note the band of cold water that wraps around the eastern side of the ring in Plates 1b and 1c. Such streamers are commonly observed in ring–shelf break current interactions [*Halliwell and Mooers*, 1979] and can transport a significant amount of shelf water offshore [*Bisagni*, 1983]. In our case, however, the streamer most likely consists only of near-surface water and does not have appreciable transport, since the volume flux of the jet is the same for both the trough and crest. Instead, the bulk of the shelf break current appears to follow the trough as indicated in Plate 1c.

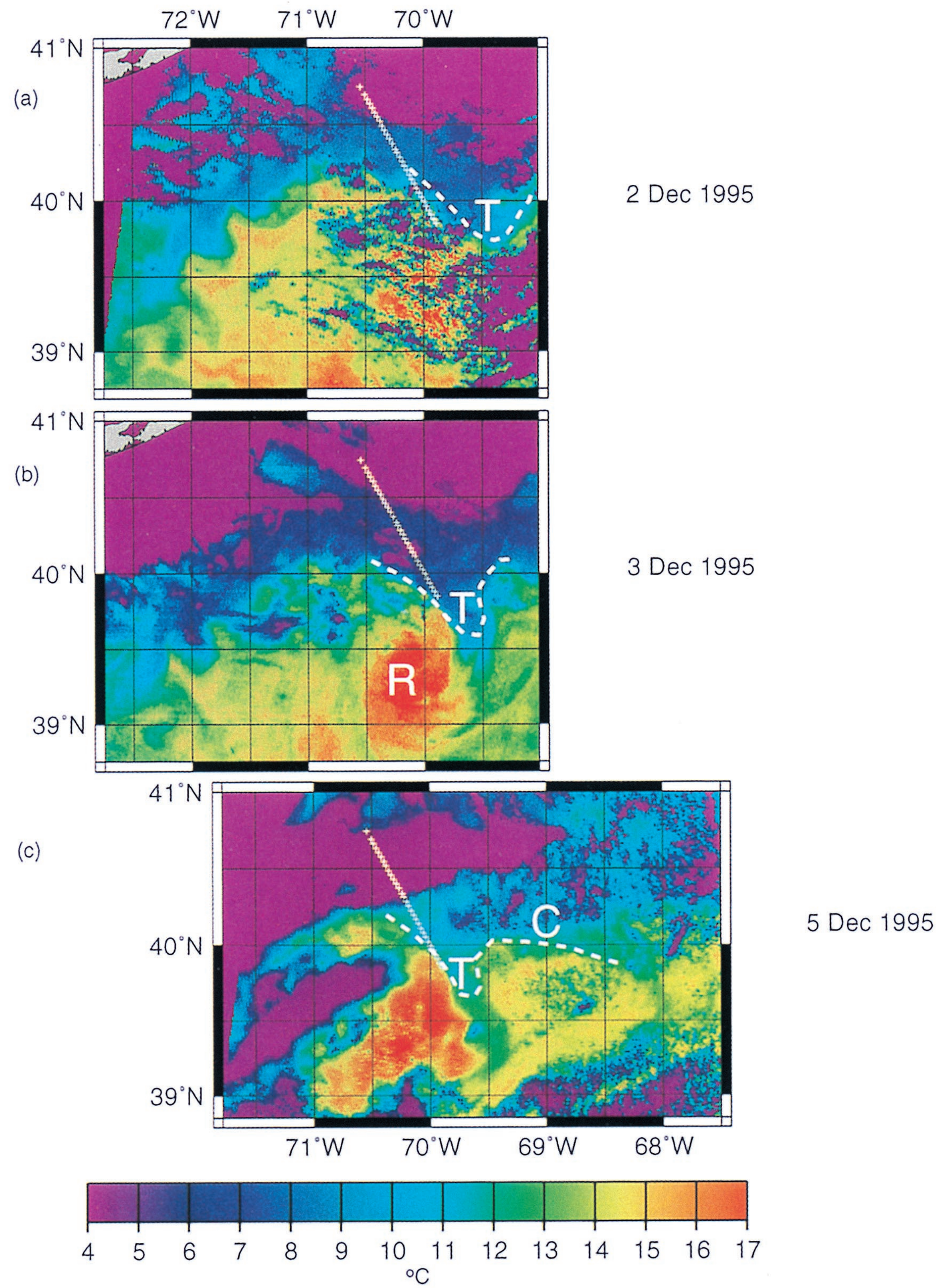


**Plate 1.** AVHRR sea surface temperature images for the PRIMER region, near the time of the cruise. The data were processed using a split-window algorithm (which removes water vapor effects); the temperatures are absolute Celsius. The hydrographic track is indicated by white crosses. (a) December 2, 1997. The location of the trough upstream of the PRIMER line is indicated by the dashed line and is labeled T. (b) December 3, 1997. The trough is indicated as in Plate 1a, and the nearby ring is labeled R. (c) December 5, 1997. The trough and following crest are shown, labeled T and C, respectively.

## 6. Summary

We have elucidated both the structure and dynamics of a meander in the shelf break current south of New England, using a combination of in situ measurements and AVHRR images. Two wintertime hydrographic/ADCP crossings of the current, separated by 3 days, sampled vastly different states of the jet, which are likely the opposite phases of a meander. In the first section the current is strong and convergent, with the core of the jet flowing along the isobaths; 3 days later, the flow is significantly weaker and divergent, with the core again aligned with the bathymetry. The Rossby number in the two cases differs by more than a factor of 2. This in turn leads to large changes in the potential vorticity structure of the current in the two realizations and suggests that the flow is highly nonlinear in the convergent state while nearly linear during its divergent phase. (This is not to say that the flow cannot be nonlinear in a crest, just not the broad crest we observed.)

Using a carefully constructed $T$-$S$ relationship from the CTD data of the second crossing, which accurately captures the strength of the shelf break front, we converted the XBT data of the first crossing into a synthesized salinity and density section. This enabled us to compute the thermal wind fields of the two sections and compare them to the ADCP-derived velocity fields. This comparison implied that a significant ageostrophic component is present during the first crossing when the flow is strong but that the current is geostrophically balanced in the weaker state during the second crossing. The available AVHRR data show the presence of a deep trough whose leading edge was sampled by the first crossing, consistent with the strong convergence measured at that time. The observed radius of curvature from the AVHRR image agrees with that predicted from gradient wind, explaining the measured ageostrophic signal. By contrast, the second crossing appears to have sampled a broad, trailing crest, in concert with the weak, divergent jet observed in the ADCP velocity field. The much larger radius of curvature based on the AVHRR image implies a minimal ageostrophic component in this case, also as observed. The conclusion is that the first crossing sampled a highly nonlinear meander trough governed by gradient wind dynamics, while the second crossing sampled a broad meander crest in approximate geostrophic balance.

These results have offered the first such quantitative glimpse of a finite amplitude meander of the shelf break current. In this case the steepening of the trough was likely influenced by the nearby Gulf Stream ring. Future work needs to address both the impact of rings and the full three-dimensional structure of such shelf break frontal variability. Results from the two main PRIMER field studies will shed light on both these issues.

**Acknowledgments.** The authors wish to acknowledge the helpful insights of Glen Gawarkiewicz, who was consulted constantly during this work. We are thankful to the crew of R/V *Endeavor* for a highly successful cruise. The National Oceanic and Atmospheric Association Coastwatch program provided the AVHRR imagery data. This work was supported by ONR contract N00014-95-1-0575 as part of the Shelfbreak PRIMER experiment.

## References

Beardsley, R. C., and C. N. Flagg, The water structure, mean currents, and shelf/slope water front on the New England continental shelf, *Mem. Soc. R. Sci. Liege Collect.*, *6*, 209–225, 1976.

Bisagni, J. J., Lagrangian current measurements within the eastern margin of a warm-core Gulf Stream ring, *J. Phys. Oceanogr.*, *13*, 709–715, 1983.

Bower, A. S., Potential vorticity balances and horizontal divergence along particle trajectories in Gulf Stream meanders east of Cape Hatteras, *J. Phys. Oceanogr.*, *19*, 1669–1681, 1989.

Burrage, D. M., and R. W. Garvine, Supertidal frequency internal waves on the continental shelf south of New England, *J. Phys. Oceanogr.*, *17*, 808–819, 1987.

Burrage, D. M., and R. W. Garvine, Summertime hydrography at the shelfbreak front in the Middle Atlantic Bight, *J. Phys. Oceanogr.*, *18*, 1309–1319, 1988.

Chapman, D. C., and R. C. Beardsley, On the origin of shelf water in the Middle Atlantic Bight, *J. Phys. Oceanogr.*, *19*, 384–391, 1989.

Condie, S. A., Formation and stability of shelf break fronts, *J. Geophys. Res.*, *98*, 12,405–12,416, 1993.

Flagg, C. N., and R. C. Beardsley, On the stability of the shelf-water/slope-water front south of New England, *J. Geophys. Res.*, *83*, 4623–4631, 1978.

Garvine, R. W., K. C. Wong, G. G. Gawarkiewicz, R. K. McCarthy, R. W. Houghton, and F. Aikman III, The morphology of shelf break eddies, *J. Geophys. Res.*, *93*, 15,593–15,607, 1988.

Gawarkiewicz, G., Linear stability models of shelf break fronts, *J. Phys. Oceanogr.*, *21*, 471–488, 1991.

Gawarkiewicz, G., T. G. Ferdelman, T. M. Church, and G. W. Luther III, Shelf break frontal structure on the continental shelf north of Cape Hatteras, *Cont. Shelf Res.*, *16*, 1751–1773, 1996.

Halliwell, G. R., and C. N. K. Mooers, The space-time structure and variability of the shelf water–slope water and Gulf Stream surface temperature fronts and associated warm-core eddies, *J. Geophys. Res.*, *84*, 7707–7725, 1979.

Holton, J. R., *An Introduction to Dynamic Meteorology*, 391 pp., Academic, New York, 1979.

Houghton, R. W., D. B. Olson, and P. J. Celone, Observation of an anticyclonic eddy near the continental shelf break south of New England, *J. Phys. Oceanogr.*, *16*, 60–71, 1986.

Houghton, R. W., F. Aikman, and H. W. Ou, Shelf-slope frontal structure and cross-shelf exchange at the New England shelf-break, *Cont. Shelf Res.*, *8*, 687–710, 1988.

Hummon, J., and T. Rossby, Spatial and temporal evolution of a Gulf Stream crest—warm core ring interaction, *J. Geophys. Res.*, *103*, 2795–2809, 1998.

Johns, E., D. R. Watts, and H. T. Rossby, A test of geostrophy in the Gulf Stream, *J. Geophys. Res.*, *94*, 3211–3222, 1989.

Joyce, T. M., J. K. B. Bishop, and O. B. Brown, Observations of offshore shelf water transport induced by a warm-core ring, *Deep Sea Res., Part A*, *39*, suppl. 1, S97–S113, 1992.

Linder, C. A., and G. G. Gawarkiewicz, A climatology of the shelf break front in the Middle Atlantic Bight, *J. Geophys. Res.*, *103*, 18,405–18,423, 1998.

Moody, J. A., et al., Atlas of tidal elevation and current observations on the Northeast American continental shelf and slope of North America, *U.S. Geol. Surv. Bull.*, *1611*, 122 pp., 1984.

Morgan, D. T., Linear instability of the shelfbreak front off the southern flank of Georges Bank, Ph.D. thesis, 190 pp., Thayer Sch. of Eng., Dartmouth Coll., 1997.

Ou, H. W., Wind-driven motion near a shelf-slope front, *J. Phys. Oceanogr.*, *14*, 985–993, 1984.

Petrie, B., and K. Drinkwater, Temperature and salinity variability on the Scotian Shelf and in the Gulf of Maine 1945–1990, *J. Geophys. Res.*, *98*, 20,079–20,089, 1993.

Ramp, S. R., R. C. Beardsley, and R. Legeckis, An observation of frontal wave development on a shelf slope/warm core ring front near the shelf break south of New England, *J. Phys. Oceanogr.*, *13*, 907–912, 1983.

Spall, M. A., Frontogenesis, subduction, and cross-front exchange at upper ocean fronts, *J. Geophys. Res.*, *100*, 2543–2557, 1995.

Spall, M. A., Baroclinic jets in confluent flow, *J. Phys. Oceanogr.*, *27*, 1054–1071, 1997.

Wright, W. R., The limits of shelf water south of Cape Cod, 1941 to 1972, *J. Mar. Res.*, *34*, 1–14, 1976.

M. J. Caruso, T. K. McKee, R. S. Pickart, J. E. Przystup, and D. J. Torres, Woods Hole Oceanographic Institution, Woods Hole, MA 02543. (rpickart@whoi.edu)

(Received July 18, 1997; revised May 27, 1998;
accepted September 10, 1998.)